From gymnastics to virtual nonholonomic constraints: energy injection, dissipation, and regulation for the acrobot

Adan Moran-MacDonald, *Member, IEEE*, Manfredi Maggiore, *Member, IEEE**, and Xingbo Wang

***Abstract*— In this article we study virtual nonholonomic constraints, which are relations between the generalized coordinates and momenta of a mechanical system that can be enforced via feedback control. We design a constraint which emulates gymnastics giant motion in an acrobot, and prove that this constraint can inject or dissipate energy based on the sign of a design parameter. The proposed constraint is tested both in simulation and experimentally on a real-world acrobot, demonstrating highly effective energy regulation properties and robustness to a variety of disturbances.**

***Index Terms*— energy regulation, virtual nonholonomic constraints, acrobot, gymnastics.**

I. Introduction

In gymnastics terminology, a "giant" is the motion a gymnast performs to achieve full rotations around a horizontal bar [15]. A gymnast will begin by hanging at rest, then swing their legs appropriately to gain energy over time. The authors of [17] modelled the gymnast as a variable length pendulum, and studied how the pendulum's length changes as a function of the gymnast's limb angle. Labelling the pendulum length by r and the gymnast's body orientation by θ, they observed experimentally that the value $\dot{r}/r$ has the biggest impact on the magnitude of energy injection. After testing several gymnasts under a variety of experimental conditions, they discovered that the peak value of $\dot{r}/r$ occurred at the same fixed value of $\dot{\theta}/\theta$ for all gymnasts. In other words, gymnasts appear to move their legs as a function of their body angle and velocity when performing giants; doing so allows them to gain energy and rotate around the bar.

While the simplest model of a gymnast is the variable-length pendulum, a more realistic model is the two-link acrobot (Figure 1). Here, the top link represents the torso while the bottom link represents the legs. The acrobot is actuated exclusively at the centre joint (the hip). To solve the swingup problem, one might begin by designing a leg controller which provably injects energy into the acrobot, so that the resulting motion mimics that of a human performing a giant.

Previous attempts at acrobot giant generation have involved trajectory tracking, partial feedback linearization, or other energy-based methods (see [5], [13], [14], [23]). While all these approaches succeed at making the acrobot rotate around the bar, none of them use the results of [17]. That is, none of these leg controllers track a function of the acrobot's body angle and velocity. In 2016, Wang designed a controller which tracked the body angle and an *estimate* of the velocity, but not the velocity itself [21]. His approach was a preliminary version of a recent technique know as the method of virtual nonholonomic constraints.

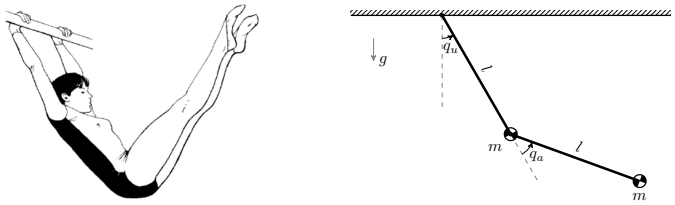

Fig. 1: A simplified two-link acrobot as a model for a gymnast. Image modified from [21].

Virtual nonholonomic constraints (VNHCs) have been used for human-robot interaction [1], [18], [19], error-reduction on time-delayed systems [20], and they have shown marked improvements to the field of bipedal locomotion [2], [4], [6]. Indeed, they produce more robust walking motion in biped robots than other virtual constraints which do not depend on velocity [7]. In particular, VNHCs may be capable of injecting and dissipating energy from a system in a robust manner, all while producing realistic biological motion.

In this article, we design a virtual nonholonomic constraint which provably injects energy into the acrobot through human-like giant motion. We will provide simulations to show how one can use VNHCs to regulate energy, along with experimental results which demonstrate the robustness of this behaviour to model uncertainty, sensor noise, and a variety of external disturbances.

Notation: We use the following notation and terminology in this article. The $n \times n$ identity matrix is denoted I_n, and the $n \times m$ matrix of zeros is denoted $\mathbf{0}_{n\times m}$. A matrix $A \in \mathbb{R}^{n\times m}$ is *right semi-orthogonal* if $AA^\mathsf{T} = I_n$ and is *left semi-orthogonal* if $A^\mathsf{T}A = I_m$. For $A \in \mathbb{R}^{n\times m}$ and $B \in \mathbb{R}^{p\times m}$, we define $[A;B] \in \mathbb{R}^{(n+p)\times m}$ as the matrix obtained by stacking A on top of B. Given $\sigma_1, \ldots, \sigma_n \in \mathbb{R}$, we define $\operatorname{diag}(\sigma_1, \ldots, \sigma_n) \in \mathbb{R}^{n\times n}$ as the diagonal matrix whose value at row i, column i is σ_i. For $T > 0$, the set of

Manuscript submitted for review on October 12, 2021.

A. Moran-MacDonald (e-mail: adan.moran@mail.utoronto.ca) and M. Maggiore (e-mail: maggiore@control.utoronto.ca) are with the Department of Electrical and Computer Engineering, University of Toronto, ON, Canada.

X. Wang is with ??? (e-mail: ???).

real numbers modulo T is denoted $[\mathbb{R}]_T$, with $[\mathbb{R}]_\infty := \mathbb{R}$. The gradient of a matrix-valued function $A : \mathbb{R}^m \to \mathbb{R}^{n\times n}$ is the block matrix of stacked partial derivatives, $\nabla_x A := [\partial A/\partial x_1; \cdots ; \partial A/\partial x_m] \in \mathbb{R}^{nm\times n}$. Given two matrices $A \in \mathbb{R}^{n\times m}$ and $B \in \mathbb{R}^{r\times s}$, the Kronecker product (see [16]) is the matrix $A \otimes B \in \mathbb{R}^{nr\times ms}$ defined as

$$A \otimes B = \begin{bmatrix} A_{1,1}B & \cdots & A_{1,m}B \\ \vdots & \ddots & \vdots \\ A_{n,1}B & \cdots & A_{n,m}B \end{bmatrix}. \tag{1}$$

The Poisson bracket [9] between the functions $f(q,p)$ and $g(q,p)$ is

$$[f,g] := \sum_{i=1}^{n} \frac{\partial f}{\partial p_i}\frac{\partial g}{\partial q_i} - \frac{\partial f}{\partial q_i}\frac{\partial g}{\partial p_i}. \tag{2}$$

The Kronecker delta δ_i^j is 1 if $i = j$ and 0 otherwise. Finally, we say a function $\Delta(I)$ is $O(I^2)$ if $\lim_{I\to 0} \Delta(I)/I = 0$.

II. Problem Formulation

We will use the simplified acrobot model in Figure 1, where we assume the torso and leg rods are of equal length l with equal point masses m at the tips. The acrobot's configuration is described in generalized coordinates (q_u, q_a) on the configuration manifold $\mathcal{Q} = \mathbb{S}^1 \times \mathbb{S}^1$, where q_u is unactuated and q_a is actuated. We ignore dissipative forces in this model.

The acrobot has inertia matrix M, potential function V (with respect to the horizontal bar), and input matrix B given as follows:

$$M(q) = \begin{bmatrix} ml^2\,(3 + 2\cos(q_a)) & ml^2\,(1 + \cos(q_a)) \\ ml^2\,(1 + \cos(q_a)) & ml^2 \end{bmatrix}, \tag{3}$$

$$V(q) = -mgl\,(2\cos(q_u) + \cos(q_u + q_a)), \tag{4}$$

$$B = [0; 1]. \tag{5}$$

For reasons that will become clear later in this article, we use Hamiltonian mechanics to derive the dynamics of the acrobot. For this we require the conjugate of momenta, $p = (p_u, p_a) = M(q)\dot{q}$. The dynamics of the acrobot in (q,p) coordinates are given in (6). For shorthand, we write $c_u := \cos(q_u)$, $c_a := \cos(q_a)$, and $c_{ua} := \cos(q_u + q_a)$; likewise, $s_u := \sin(q_u)$, $s_a := \sin(q_a)$, and $s_{ua} := \sin(q_u + q_a)$.

$$\mathcal{H}(q,p) = \frac{1}{2}p^\mathsf{T} M^{-1}(q)p - mgl\,(2c_u + c_{ua}), \tag{6}$$

$$\begin{cases} \dot{q} = M^{-1}(q)p, \\ \dot{p}_u = -mgl\,(2s_u + s_{ua}), \\ \dot{p}_a = -\frac{1}{2}p^\mathsf{T}\nabla_{q_a} M^{-1}(q)p - mgl s_{ua} + \tau. \end{cases}$$

The control input is a force $\tau \in \mathbb{R}$ affecting only the dynamics of p_a, representing a torque acting on the hip joint.

Our goal is to design a smooth function $f : \mathbb{S}^1 \times \mathbb{R} \to \mathbb{S}^1$ such that the relation $q_a = f(q_u, p_u)$ for system (6) can be enforced asymptotically via feedback control (in Section III we call this a virtual nonholonomic constraint). We will further require that the dynamics of the acrobot, when the relation holds, gain or lose energy in a sense that will be defined precisely in Section IV-A.

III. Preliminaries on VNHCs

Before embarking on the design problem, we must summarize the relevant theory of virtual nonholonomic constraints for a class of mechanical systems we call "simply actuated Hamiltonian systems". The results we provide in Section III-B are not novel: they are a special case of the results in [6].

A. Simply Actuated Hamiltonian Systems

Take a mechanical system modelled with generalized coordinates $q = (q_1, \ldots, q_n)$ on a configuration manifold $\mathcal{Q} = [\mathbb{R}]_{T_1} \times \cdots \times [\mathbb{R}]_{T_n}$, where $T_i = 2\pi$ if q_i is an angle and $T_i = \infty$ if q_i is a displacement. The corresponding generalized velocities are $\dot{q} = (\dot{q}_1, \ldots, \dot{q}_n) \in \mathbb{R}^n$.

Suppose this system has Lagrangian $\mathcal{L}(q,\dot{q}) = 1/2\ \dot{q}^T D(q)\dot{q} - P(q)$, where the potential energy $P : \mathcal{Q} \to \mathbb{R}$ is smooth, and the inertia matrix $D : \mathcal{Q} \to \mathbb{R}^{n\times n}$ is smooth and positive definite for all $q \in \mathcal{Q}$. The *conjugate momentum* to q is the vector $p := \partial\mathcal{L}/\partial\dot{q} = D(q)\dot{q} \in \mathbb{R}^n$. As per [9], the *Hamiltonian* of the system in (q,p) coordinates is

$$\mathcal{H}(q,p) = \frac{1}{2}p^\mathsf{T} D^{-1}(q)p + P(q), \tag{7}$$

with dynamics

$$\begin{cases} \dot{q} = \nabla_p \mathcal{H}, \\ \dot{p} = -\nabla_q \mathcal{H} + B(q)\tau, \end{cases} \tag{8}$$

where $\tau \in \mathbb{R}^k$ is a vector of generalized input forces and the input matrix $B : \mathcal{Q} \to \mathbb{R}^{n\times k}$ is full rank for all $q \in \mathcal{Q}$. If $k < n$, we say the system is *underactuated* with degree of underactuation $(n - k)$.

Using the matrix Kronecker product, it is easy to show that (8) expands to

$$\begin{cases} \dot{q} = D^{-1}(q)p, \\ \dot{p} = -\frac{1}{2}(I_n \otimes p^\mathsf{T})\nabla_q D^{-1}(q)p - \nabla_q P(q) + B(q)\tau. \end{cases}$$

Because τ is transformed by $B(q)$, it is not obvious how any particular input force τ_i affects the system. As a first step in addressing this problem, we make the following assumptions.

Assumption 1: The input matrix $B(q) \equiv B \in \mathbb{R}^{n\times k}$ is constant and has full rank $k < n$.

When $\mathcal{Q} = \mathbb{R}^n$, the above assumption allows us to define a canonical coordinate transformation of (7) which decouples the input forces. To define this transformation we will make use of the following lemma.

Lemma 1: Suppose Assumption 1 holds. Then there exists a nonsingular matrix $\hat{T} \in \mathbb{R}^{k\times k}$ so that the regular feedback transformation

$$\tau = \hat{T}\hat{\tau}$$

has a new input matrix $\hat{B}$ for $\hat{\tau}$ which is left semi-orthogonal.

Proof: Since B is constant and full rank, it has a singular value decomposition $B = U^\mathsf{T}\Sigma V$ where $\Sigma = [\mathrm{diag}\,(\sigma_1, \ldots, \sigma_k); \mathbf{0}_{(n-k)\times k}]$, $\sigma_i > 0$, and $U \in R^{n\times n}$, $V \in \mathbb{R}^{k\times k}$ are unitary matrices [3]. Defining $T = \mathrm{diag}\,(1/\sigma_1, \ldots, 1/\sigma_k)$ and assigning the regular feedback transformation $\tau = VT\hat{\tau}$ yields a new input matrix $\hat{B} = BVT$ for $\hat{\tau}$ such that $\hat{B}^\mathsf{T}\hat{B} = T^\mathsf{T}\Sigma^\mathsf{T}\Sigma T = I_k$. ■

In light of Lemma 1, there is no loss of generality in assuming that the input matrix B is left semi-orthogonal, which means that B^T is right semi-orthogonal. Now, let $\mathbf{B} := [B^\perp; B^\mathsf{T}]$ where $B^\perp \in \mathbb{R}^{(n-k)\times k}$ is a full-rank left annihilator of B, i.e., $B^\perp B = \mathbf{0}_{(n-k)\times k}$. Since B is constant, such a $B^\perp$ exists and $\mathbf{B}$ is invertible.

The following theorem requires that $\mathcal{Q} = \mathbb{R}^n$ so that the coordinate transformation is well defined.

Theorem 1: Take the Hamiltonian system (7) with configuration manifold $\mathcal{Q} = \mathbb{R}^n$ and suppose Assumption 1 holds. The coordinate transformation $\left(\tilde{q} = (\mathbf{B}^\mathsf{T})^{-1}q, \tilde{p} = \mathbf{B}p\right)$ is a canonical transformation and the resulting dynamics are given by

$$\mathcal{H}(\tilde{q},\tilde{p}) = \frac{1}{2}\tilde{p}^\mathsf{T}M^{-1}(\tilde{q})\tilde{p} + V(\tilde{q}), \tag{9}$$

$$\begin{cases} \dot{\tilde{q}} = M^{-1}(\tilde{q})\tilde{p}, \\ \dot{\tilde{p}} = -\frac{1}{2}(I_n \otimes \tilde{p}^\mathsf{T})\nabla_{\tilde{q}}M^{-1}(\tilde{q})\tilde{p} \\ \qquad\quad - \nabla_{\tilde{q}}V(\tilde{q}) + \begin{bmatrix}\mathbf{0}_{(n-k)\times k} \\ I_k\end{bmatrix}\tau, \end{cases}$$

where $M^{-1}(\tilde{q}) := (\mathbf{B}^\mathsf{T})^{-1}D^{-1}(\mathbf{B}^\mathsf{T}\tilde{q})\mathbf{B}^{-1}$ and $V(\tilde{q}) := P(\mathbf{B}^\mathsf{T}\tilde{q})$.

Proof: Since $\mathbf{B}$ is constant, this transformation satisfies $\partial\tilde{q}_i/\partial p_j = \partial\tilde{p}_i/\partial q_j = 0$ for all $i,j \in \{1,\dots,n\}$. This implies the Poisson brackets $[\tilde{q}_i,\tilde{q}_j]$ and $[\tilde{p}_i,\tilde{p}_j]$ are both zero. Then, one can show that $[\tilde{p}_i,\tilde{q}_j] = (\mathbf{B}^\mathsf{T})^{-1}_i(\mathbf{B}^\mathsf{T})_j = \delta^j_i$. By (45.10) in [9], this is a canonical transformation and the new Hamiltonian is $\mathcal{H}(\mathbf{B}^\mathsf{T}\tilde{q}, \mathbf{B}^{-1}\tilde{p})$. Finally, since $\dot{\tilde{p}} = \mathbf{B}\dot{p}$, the input matrix for the system in $(\tilde{q},\tilde{p})$ coordinates is $\mathbf{B}B = [\mathbf{0}_{(n-k)\times k}; I_k]$, which proves the theorem. ∎

We call the $(\tilde{q},\tilde{p})$ coordinates *simply actuated coordinates*, and we call any Hamiltonian system whose input matrix is $[\mathbf{0}_{(n-k)\times k}; I_k]$ a *simply actuated Hamiltonian system*. The first $(n-k)$ configuration variables in $\tilde{q}$, labelled q_u, are the *unactuated coordinates*; the remaining k configuration variables, labelled q_a, are the *actuated coordinates*. The corresponding (p_u, p_a) in $\tilde{p}$ are the *unactuated* and *actuated momenta*, respectively.

In this article we focus on the acrobot which, despite having a configuration manifold which is not $\mathbb{R}^n$, is already a simply actuated Hamiltonian system.

B. Virtual Nonholonomic Constraints

Griffin and Grizzle [4] were the first to define relative degree two nonholonomic constraints which can be enforced through state feedback. Horn *et al.* later extended their results in [6] to derive the constrained dynamics for a certain class of mechanical systems. These researchers made use of the unactuated conjugate momentum, but they developed their results in the Lagrangian framework. In particular, they focused on Lagrangian systems with degree of underactuation one. We will now present a special case of [6] for simply actuated Hamiltonian systems, so that the theory we apply to the acrobot is provided in its clearest form. After we finish this summary we will clarify the relationship between our material and that of [6].

The rest of this section refers to the simply actuated system (9). For simplicity of notation, we relabel $(\tilde{q},\tilde{p})$ to (q,p). We assume henceforth that $(q,p) \in \mathcal{Q}\times\mathbb{R}^n$.

Definition 1: A *virtual nonholonomic constraint* (VNHC) *of order* k is a relation $h(q,p) = 0$ where $h : \mathcal{Q}\times\mathbb{R}^n \to \mathbb{R}^k$ is C^2, $\operatorname{rank}([dh_q,\, dh_p]) = k$ for all $(q,p) \in h^{-1}(0)$, and there exists a feedback controller $\tau(q,p)$ rendering the *constraint manifold* Γ invariant, where

$$\Gamma = \{(q,p) \mid h(q,p) = 0, dh_q\dot{q} + dh_p\dot{p} = 0\}. \tag{10}$$

The constraint manifold is a $2(n-k)$-dimensional closed embedded submanifold of $\mathcal{Q}\times\mathbb{R}^n$. A VNHC thereby allows us to study a reduced-order model of the system: it reduces the original $2n$ differential equations to $2(n-k)$ equations. In particular, if the mechanical system has degree of underactuation one, i.e., $k = (n-1)$, the constraint manifold is *always* two-dimensional.

In order to enforce the constraint $h(q,p) = 0$, we want to asymptotically stabilize the set Γ. To see when this is possible, let us define the error output $e = h(q,p)$. If any component of e_i has relative degree 1, we may not be able to stabilize Γ: we can always guarantee $e_i \to 0$, but not necessarily $\dot{e}_i \to 0$. It is for this reason that we define the following special type of VNHC.

Definition 2: A VNHC $h(q,p) = 0$ of order k is *regular* if the output $e = h(q,p)$ is of relative degree $\{2,2.\dots,2\}$ everywhere on the constraint manifold Γ.

The authors of [4], [6] observed that relations which use only the unactuated conjugate momentum often have vector relative degree $\{2,\dots,2\}$. Indeed, we shall now prove that regular constraints cannot depend on the actuated momentum.

To ease notation in the rest of this section, we use the following shorthand:

$$\mathcal{A}(q,p_u) := dh_q(q,p_u)M^{-1}(q), \tag{11}$$

$$\mathcal{M}(q,p) := (I_{n-k}\otimes p^\mathsf{T})\nabla_{q_u}M^{-1}(q). \tag{12}$$

Theorem 2: A relation $h(q,p) = 0$ for system (9) is a regular VNHC of order k if and only if $dh_{p_a} = \mathbf{0}_{k\times k}$ and the decoupling matrix

$$H(q,p) := \left(\mathcal{A}(q,p_u) - dh_{p_u}\mathcal{M}(q,p)\right)\begin{bmatrix}\mathbf{0}_{(n-k)\times k} \\ I_k\end{bmatrix}, \tag{13}$$

is invertible everywhere on the constraint manifold Γ.

Proof: Let $e = h(q,p) \in \mathbb{R}^k$. If $dh_{p_a} \neq \mathbf{0}_{k\times k}$ for some $(q,p) \in \Gamma$, then τ appears in $\dot{e}$ and the VNHC is not of relative degree $\{2,\dots,2\}$. Suppose now that $dh_{p_a} = \mathbf{0}_{k\times k}$. Then $\dot{e} = \mathcal{A}(q,p_u)p - dh_{p_u}\left(1/2\ \mathcal{M}(q,p)p + \nabla_{q_u}V(q)\right)$. Taking one further derivative provides $\ddot{e} = (\star) - dh_{p_u}\left(1/2\ d/dt\left(\mathcal{M}(q,p)p\right)\right) + \mathcal{A}(q,p_u)[\mathbf{0}_{(n-k)\times k}; I_k]\tau$, where $(\star)$ is a continuous function of q and p. One can further show that $dh_{p_u}\left(1/2\ d/dt\ \left(\mathcal{M}(q,p)p\right)\right) = (\star) + dh_{p_u}\mathcal{M}(q,p)[\mathbf{0}_{(n-k)\times k}; I_k]\tau$. Hence, $\ddot{e}$ has the form $\ddot{e} = E(q,p) + H(q,p)\tau$ for appropriate E. From the definition of regularity, the VNHC h is regular when e is of relative degree $\{2,\dots,2\}$, which is true if and only if the matrix $H(q,p)$ premultiplying τ is nonsingular. This proves the theorem. ∎

Under additional mild conditions (see [10]), a regular VNHC of order k can be stabilized by the input-output feedback

linearizing controller

$$\tau(q,p) = -H^{-1}(q,p)\left(E(q,p) + k_p e + k_d \dot{e}\right), \tag{14}$$

where $k_p, k_d > 0$ are control parameters which can be tuned on the resulting error dynamics $\ddot{e} = -k_p e - k_d \dot{e}$.

In Section IV we will enforce a regular constraint on the acrobot of the form $h(q,p) = q_a - f(q_u, p_u)$, where the actuators track a function of the unactuated variables. Regular constraints of this form always meet the mild conditions from [10], and hence we can stabilize the constraint manifold using (14). Since q_a is constrained to be a function of the unactuated variables, intuition tells us the constrained dynamics should be parameterized by (q_u, p_u). Unfortunately, $\dot{q}_u$ depends on p_a, and for general systems one cannot solve explicitly for p_a in terms of (q_u, p_u) because the $\dot{p}$ dynamics contain the coupling term $(I_n \otimes p^\mathsf{T})\nabla_q M(q)p$. We now introduce an assumption which allows us to solve for p_a as a function of (q_u, p_u), which in turn allows us to explicitly solve for the constrained dynamics.

Assumption 2: The inertia matrix does not depend on the unactuated coordinates, i.e., $\nabla_{q_u} M(q) = \mathbf{0}_{n(n-k)\times n}$.

Theorem 3: Let $\mathcal{H}$ be a Hamiltonian system in simply actuated form (9) satisfying Assumption 2. Let $h(q,p_u) = q_a - f(q_u,p_u)$ be a regular VNHC of order k with constraint manifold Γ. Then the constrained dynamics are given by

$$\left.\begin{aligned} \dot{q}_u &= \begin{bmatrix} I_{(n-k)} & \mathbf{0}_{(n-k)\times k}\end{bmatrix} M^{-1}(q)p \\ \dot{p}_u &= -\nabla_{q_u} V(q) \end{aligned}\right| \begin{aligned} q_a &= f(q_u,p_u) \\ p_a &= g(q_u,p_u) \end{aligned}, \tag{15}$$

where

$$g(q_u,p_u) := \left(\mathcal{A}(q,p_u)\begin{bmatrix}\mathbf{0}_{(n-k)\times k} \\ I_k\end{bmatrix}\right)^{-1} \cdot \Big(dh_{p_u}\nabla_{q_u}V(q) - \mathcal{A}(q,p_u)\begin{bmatrix} I_{(n-k)} \\ \mathbf{0}_{k\times(n-k)}\end{bmatrix} p_u \Big)\Big|_{q_a = f(q_u,p_u)}. \tag{16}$$

Proof: Setting $e = h(q,p_u)$ and using Assumption 2, we find that $\dot{e} = \mathcal{A}(q,p_u)p - dh_{p_u}\nabla_{q_u}V(q)$. Notice that $\mathcal{A}(q,p_u)p = \mathcal{A}(q,p_u)[\mathbf{0}_{(n-k)\times k}; I_k]p_a + \mathcal{A}(q,p_u)[I_{n-k}; \mathbf{0}_{k\times(n-k)}]p_u$. Since $h(q,p_u)$ is regular, $\mathcal{A}(q,p_u)[\mathbf{0}_{(n-k)\times k}; I_k]$ is invertible. Taking $e = \dot{e} = 0$, solving for p_a, and setting $q_a = f(q_u,p_u)$ completes the proof. ∎

Comparison with existing literature: Horn *et al.* provide the constrained dynamics for VNHCs in [7]. Their assumption **H2** is what we call regularity, and our requirement that one can solve for $q_a = f(q_u,p_u)$ on Γ implies their assumption **H3** holds true. The only real distinction between this section and their work is that our constrained dynamics are explicit functions of the Hamiltonian coordinates (q_u,p_u). In fact, one can show that the constrained dynamics (15) coincide with the constrained dynamics in [6, Eqn. (17)] when one chooses the special case $\theta_1 = q_u$ and $\theta_2 = p_u$. This explicit representation will be beneficial when we apply the theory of VNHCs to the acrobot.

IV. The Proposed Acrobot VNHC

The goal in this article is to design a VNHC which injects energy into the acrobot by means of a giant-like motion. Recall that the acrobot in Figure 1 has dynamics given by (6), repeated here for convenience:

$$\begin{cases} \dot{q} = M^{-1}(q)p, \\ \dot{p}_u = -mgl\left(2s_u + s_{ua}\right), \\ \dot{p}_a = -\frac{1}{2}p^\mathsf{T}\nabla_{q_a}M^{-1}(q)p - mgls_{ua} + \tau. \end{cases}$$

Since the control input τ only affects the actuated momentum, the system above is already in simply actuated form. Its state space is $\mathbb{S}^1\times\mathbb{S}^1\times\mathbb{R}\times\mathbb{R}$. We can therefore apply the theory from Section III to design a VNHC of the form $q_a = f(q_u,p_u)$ (i.e., a VNHC $h(q,p_u) = q_a - f(q_u,p_u) = 0$). Since we need the VNHC to be regular, the following proposition will be useful.

Proposition 1: Any relation $q_a = f(p_u)$ with $f \in C^2\left(\mathbb{R};\mathbb{S}^1\right)$ is a regular VNHC of order 1 for the acrobot in (6).

Proof: The decoupling matrix (13) for the acrobot evaluates to $((1+c_a)\partial_{q_u}f(q_u,p_u) + (3+2c_a))/(ml^2(2-c_a^2))$. Since $\partial_{q_u}f = 0$, this function is positive for all values of q_a, and hence is full rank 1 everywhere on the constraint manifold. ∎

To design the VNHC, we begin by examining a person on a seated swing. The person extends their legs when the swing moves forward, and retracts their legs when the swing moves backward. As the swing gains speed, the person leans their body while extending their legs higher, thereby shortening the distance from their centre of mass to the pivot and adding more energy to the swing [22].

Now imagine the person's torso is affixed to the swing's rope so they are always upright. Imagine further that the swing has no seat, allowing the person to extend their legs beneath them. This position is identical to that of a gymnast on a bar.

The acrobot's legs are rigid rods which cannot retract, so we emulate the person on a swing by pivoting the legs toward the direction of motion. Since a person lifts their legs higher at faster speeds, the acrobot's legs should pivot to an angle proportional to the swing's speed. A real gymnast cannot swing their legs in full circles, though they are usually flexible enough to raise them parallel to the floor; hence, the VNHC must restrict the leg angle q_a to lie in $[-Q_a, Q_a]$ for some $Q_a \in [\frac{\pi}{2}, \pi[$. Because the direction of motion is entirely determined by p_u, one VNHC which emulates this process is $q_a = \bar{q}_a \arctan(Ip_u)$, displayed in Figure 2. Here, $\bar{q}_a \in]0, 2Q_a/\pi]$ and $I \in \mathbb{R}$ are design parameters.

This constraint does not perfectly recreate giant motion, during which the gymnast's legs are almost completely extended [15]. It instead pivots the legs partially during rotations. However, the behaviour is similar enough that this constraint will still inject energy into the acrobot. The final VNHC is

$$h(q,p) = q_a - \bar{q}_a \arctan(Ip_u). \tag{17}$$

Recall that (q_u,p_u) denote the angle and momentum of the acrobot's torso. By Theorem 3, the constrained dynamics arising from the VNHC (17) are parameterized fully by $(q_u,p_u) \in \mathbb{S}^1 \times \mathbb{R}$. Here, (16) reduces to

$$g(q_u,p_u) = \frac{(1+c_a)p_u}{ml^2(3+2c_a)} - \frac{mgl\bar{q}_a I(2-c_a^2)(2s_u + s_{ua})}{(3+2c_a)(1+I^2p_u^2)},$$

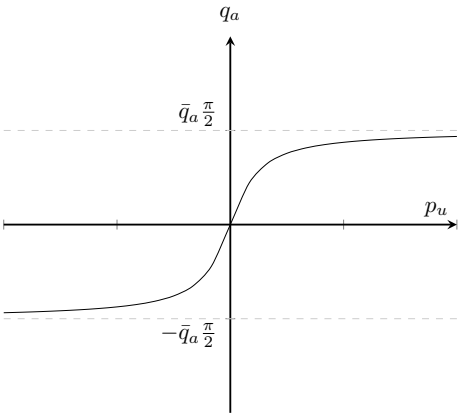

Fig. 2: The acrobot constraint $q_a = \bar{q}_a \arctan(Ip_u)$.

and the constrained dynamics (15) are

$$\begin{cases} \dot{q}_u &= \frac{(1+I^2p_u^2)p_u + m^2gl^3\bar{q}_aI(2s_u+s_{ua})(1+c_a)}{ml^2(1+I^2p_u^2)(3+2c_a)}, \\ \dot{p}_u &= -mgl(2s_u + s_{ua}), \end{cases} \tag{18}$$

subject to $q_a = \bar{q}_a \arctan(Ip_u)$. In what follows, we denote by $x = (q_u, p_u)$ the state of the constrained dynamics (18), and by $x(t, x_0)$ the solution of (18) at time t with initial condition $x(0) = x_0$. We let $x([a,b], x_0)$ denote the set $\{x(t, x_0) : t \in [a, b]\}$.

A. Energy Injection and Dissipation with the Proposed VNHC

Suppose for a moment that $I = 0$ in (17), i.e., that the legs stay fully extended. The acrobot becomes a nominal pendulum with two masses, whose total mechanical energy is

$$E(q_u, p_u) := \frac{p_u^2}{10ml^2} + 3mgl(1 - \cos(q_u)). \tag{19}$$

The function $E(q_u, p_u)$ is a first integral for the constrained dynamics (18), i.e., each solution of the constrained dynamics is confined to a level set of E, and each orbit not containing equilibria is a connected component of a level set of E. Given scalars R and $R_1 < R_2$, and letting $\# \in \{$ "$<$","$\leq$","$>$","$\geq$"$\}$, we define the following sets (see Figure 3):

$$\begin{aligned} E_R &:= \{(q_u, p_u) : E(q_u, p_u) = R\}, \\ E_{\#R} &:= \{(q_u, p_u) : E(q_u, p_u) \# R\}, \\ E_{[R_1,R_2]} &:= \{(q_u, p_u) : R_1 \leq E(q_u, p_u) \leq R_2\}. \end{aligned} \tag{20}$$

Letting $\bar{R} := E(\pi, 0)$, solutions initialized in the interior of the set $E_{\leq \bar{R}}$ correspond to *oscillations* of the pendulum, i.e., rocking motions where the pendulum does not perform full revolutions. On the other hand, for each $R > \bar{R}$, solutions initialized in the interior of the set $E_{[\bar{R},R]}$ correspond to *rotations* of the pendulum, i.e., full revolutions around the pivot point.

Now consider the case $I \neq 0$, i.e., when the acrobot is not fully extended. The constrained dynamics (18) are no longer Hamiltonian, and their solutions are no longer confined to level sets of E. In what follows, we will show that the orbits of the constrained dynamics roughly speaking gain energy or lose energy depending on the sign of the design parameter I. To be more precise in describing this energy injection or dissipation property, we next define what is an oscillation or a rotation gaining or losing energy. Intuitively, oscillations gaining energy correspond to rocking motions of the torso with increasing amplitude, while rotations gaining energy correspond to full revolutions with increasing speed. Figure 3 illustrates these concepts.

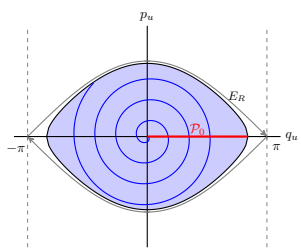

(a) The set $E_{\leq R}$ with $0 < R < \bar{R}$ and an oscillation gaining energy.

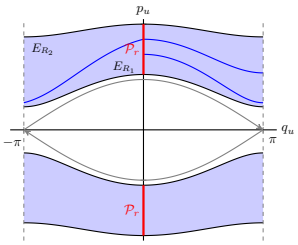

(b) The set $E_{[R_1,R_2]}$, with $\bar{R} < R_1 < R_2$, and a rotation gaining energy.

Fig. 3: Oscillations and rotations gaining energy.

We define two Poincaré sections,

$$\begin{aligned} \mathcal{P}_o &:= \{(q_u, p_u) \in E_{<\bar{R}} : q_u > 0, p_u = 0\} \\ \mathcal{P}_r &:= \{(q_u, p_u) \in E_{>\bar{R}} : q_u = 0\}. \end{aligned}$$

Consider a solution $x(t, x_0)$ of the constrained dynamics (18). We say that $x(t, x_0)$ is an *oscillation over* $[0, \bar{t}]$ if $x([0, \bar{t}], x_0) \cap \mathcal{P}_o$ is a discrete set, i.e., a set of isolated points. Similarly, $x(t, x_0)$ is a *rotation over* $[0, \bar{t}]$ if $x([0, \bar{t}], x_0) \cap \mathcal{P}_r$ is a discrete set. The isolated points mentioned above represent consecutive crossings of the Poincaré sections $\mathcal{P}_o$ and $\mathcal{P}_r$ by the solution $x(t, x_0)$ at times t_o^i, t_r^i, where $t_{o,r}^i < t_{o,r}^{i+1}$.

Letting $x_o^i(x_0) := x(t_o^i, x_0)$ and $x_r^i(x_0) := x(t_r^i, x_0)$, we say that *an oscillation over* $[0, \bar{t}]$ *gains energy (respectively, loses energy)* if the sequence $\{\|x_o^i(x_0)\|\}$ is monotonically increasing (respectively, monotonically decreasing) with i. Similarly, *a rotation over* $[0, \bar{t}]$ *gains energy (respectively, loses energy)* if the sequence $\{\|x_r^i(x_0)\|\}$ is monotonically increasing (respectively, monotonically decreasing) with i.

The next theorem states that if the design parameter I in the VNHC (17) is chosen small enough, then the constrained dynamics have oscillations gaining or losing energy, depending on the sign of I.

Theorem 4 (oscillations gaining/losing energy): Consider the constrained dynamics in (18). For each $R_1 < R_2 \in]0, \bar{R}[$, there exists $I^\star > 0$ such that for each $I \in]0, I^\star]$ (respectively, $I \in [-I^\star, 0[$) and $x_0 \in E_{[R_1,R_2]}$, there exists $\bar{t} \geq 0$ such that $x(\bar{t}, x_0) \in E_{R_2}$ (respectively, $x(\bar{t}, x_0) \in E_{R_1}$), and $x(t, x_0)$ is an oscillation gaining energy (respectively, losing energy) over $[0, \bar{t}]$.

Proof: See Section VII. ∎

The next result concerns rotations. In preparation for the theorem statement, we define

$$b(r, \theta) := \frac{5C\left(\frac{C}{\bar{q}_a}\left(18s_\theta^2 + 30c_\theta(1 - c_\theta)\right) - c_\theta r^2\right)}{|r|\sqrt{r^2 - 30m^2gl^3(1 - c_\theta)}},$$

with $C = m^2 g l^3 \bar{q}_a$, and $S(r) := \int_0^{2\pi} b(r,\theta)d\theta$.

Theorem 5 (rotations gaining/losing energy): Consider the constrained dynamics in (18), and fix R_1, R_2 such that $\bar{R} < R_1 < R_2$. Suppose there exists $\varepsilon > 0$ such that $S(r) \geq \varepsilon$ for all $r \in [(10ml^2R_1)^{1/2}, (10ml^2R_2)^{1/2}]$. Then there exists $I^\star > 0$ such that, for each $I \in]0, I^\star]$ (respectively, $I \in [-I^\star, 0[$) and $x_0 \in E_{[R_1,R_2]}$, there exists $\bar{t} \geq 0$ such that $x(\bar{t}, x_0) \in E_{R_2}$ (respectively, $x(\bar{t}, x_0) \in E_{R_1}$), and $x(t, x_0)$ is a rotation gaining energy (respectively, losing energy) over $[0, \bar{t}]$.

Proof: See Section VII. ■

Remark 1: Theorem 4 concerning oscillations gaining/losing energy states that for any set of physical parameters, the acrobot constrained by (17) will gain enough energy to exit (in finite time) a level set of the function E arbitrarily close to the boundary $E_{\bar{R}}$ separating oscillations from rotations, provided the parameter I in (17) is chosen small enough. The result is semiglobal relative to the set $E_{<\bar{R}}$ in that energy gain can be achieved on any compact subset $E_{[R_1,R_2]}$ of $E_{<\bar{R}}$ by a suitably small I. Vice versa, for small *negative* I, the oscillations will lose energy on any compact subset $E_{[R_1,R_2]}$ of $E_{<\bar{R}}$.

Theorem 5 concerning rotations relies on an assumption on the function $S(r)$ which depends on the physical parameters of the acrobot, as well as the design parameter $\bar{q}_a$. The result is otherwise analogous to Theorem 4.

Remark 2: The theorems above state that under certain conditions, if the design parameter I is chosen small enough then the acrobot will exhibit oscillations and rotations gaining energy. The oscillations will exit a compact subset of $E_{<\bar{R}}$ in finite time, while the rotations will exit a compact subset of $E_{>\bar{R}}$. Will the oscillations gaining energy eventually turn into rotations gaining energy? The theorem does not answer this question, but extensive simulations and physical experiments presented below suggest that the answer is yes.

B. Energy Regulation

One can apply the results of Theorems 4 and 5 towards energy regulation; that is, one can stabilize oscillations or rotations by appropriately toggling between injection and dissipation VNHCs, which can be achieved by changing the sign of I in (17).

Rotation Regulation: choose a desired rotation rate $p_{\text{des}} > 0$ and a hysteresis value $\delta \in [0, 1]$ such that $(1-\delta)p_{\text{des}} > \sqrt{60m^2gl^3}$. Each time the orbit crosses the p_u-axis (i.e. when $q_u = 0$), the supervisor changes which VNHC is enforced as follows:

- If $|p_u| < (1-\delta)p_{\text{des}}$, enable the injection VNHC by setting $I > 0$ in (17).
- If $|p_u| > (1+\delta)p_{\text{des}}$, enable the dissipation VNHC by replacing $I > 0$ with $-I < 0$ in (17).
- If $(1-\delta)p_{\text{des}} \leq |p_u| \leq (1+\delta)p_{\text{des}}$, extend the leg fully by setting $q_a = 0$. In simulation we assume this can be done instantaneously, though in practice this takes time.

All orbits of the acrobot initialized in $E_{<\bar{R}}$ must cross the p_u axis. The procedure above exploits this observation to stabilize a rotation even if the acrobot is initialized in $E_{<\bar{R}}$, although in this case we do not offer a theoretical guarantee (see Remark 2). While the above supervisor is designed to regulate a rotation rate, it does not impose the rotation direction.

Oscillation Regulation: Choose a desired oscillation angle $q_{\text{des}} \in]0, \pi[$ and, to avoid infinite switching, a hysteresis value $\delta \in [0, \pi/q_{\text{des}} - 1]$. An orbit in the (q_u, p_u)-plane will either cross the q_u axis if the orbit corresponds to a rocking motion, or it will cross the line $|q_u| = \pi$ if the orbit corresponds to a full revolution. When either of these occur, the supervisor does the following:

- If $|q_u| < (1-\delta)q_{\text{des}}$, enable the injection VNHC.
- If $|q_u| > (1+\delta)q_{\text{des}}$, enable the dissipation VNHC.
- If $(1-\delta)q_{\text{des}} \leq |q_u| \leq (1+\delta)q_{\text{des}}$, keep the leg extended at $q_a = 0$. This can be done continuously since $q_a = 0$ when $p_u = 0$.

Note that by the choice of δ, if the supervisor kicks in when $|q_u| = \pi$ (i.e., when the robot is rotating) then the supervisor will automatically enable the dissipation VNHC.

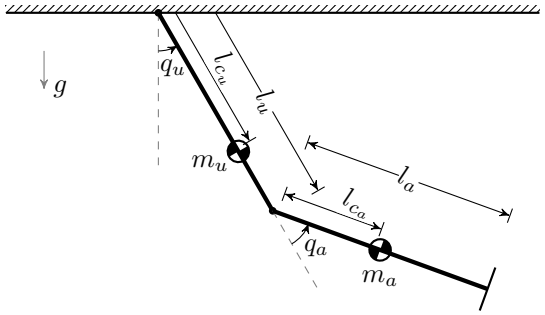

Fig. 4: The distributed mass acrobot model, represented by two weighted rods differing in both length and mass.

V. Simulation Results

In Section VI we will test the VNHC (17) on a physical acrobot. While the acrobot model used for the theoretical development assumes point-masses and links of equal lengths, the physical acrobot has distributed mass and unequal lengths. In preparation for the experiments, in this section we simulate the proposed VNHC controller on a more accurate acrobot model, depicted in Figure 4, with distributed mass and unequal link lengths. Let

$$\begin{aligned} m_{11}(q) :=& m_a l_u^2 + 2m_a l_u l_{c_a}\cos(q_a) + m_a l_{c_a}^2 + m_u l_{c_u}^2 \\ &+ J_u + J_a, \\ m_{12}(q) :=& m_a l_{c_a}^2 + m_a l_u l_{c_a}\cos(q_a) + J_a, \\ m_{22}(q) :=& m_a l_{c_a}^2 + J_a, \end{aligned}$$

where J_u and J_a are the moments of inertia of the torso and leg links respectively, and all other parameters are illustrated in Figure 4. The distributed mass acrobot has inertia matrix

$$M(q) = \begin{bmatrix} m_{11}(q) & m_{12}(q) \\ m_{12}(q) & m_{22}(q) \end{bmatrix},$$

and potential function

$$V(q) = g\big(m_a l_{c_a}(1 - c_{ua}) + (m_a l_u + m_u l_{c_u})(1 - c_u)\big).$$

TABLE I: Physical parameters for the real acrobot.

m_u (kg)	m_a (kg)	l_u (m)	l_a (m)	l_{c_u} (m)	l_{c_a} (m)	J_u (kg·m^2)	J_a (kg·m^2)	g (m/s^2)
0.2112	0.1979	0.148	0.145	0.073	0.083	0.00129	0.00075	9.81

Theorems 4 and 5 make use of the mechanical energy (19) of the nominal pendulum obtained by setting $I = 0$ in (17). Using the parameters in Table I and the inertia matrix and potential function given above, we get the mechanical energy of the nominal pendulum with $I = 0$:

$$E(q_u, p_u) \approx 396.5501 p_u^2 + 0.5997(1 - \cos(q_u)).$$

This is the function we use in interpreting the simulation results presented next.

We will now simulate the effects of constraining the physical acrobot with the VNHC (17), thereby demonstrating that VNHCs are robust to model mismatch. According to Theorems 4 and 5, the control parameter I must be "small" for the VNHC (17) to inject (or dissipate) energy into the simplified acrobot. The theorems do not specify how small $|I|$ must be; while we could make it arbitrarily small in simulations, we will eventually implement this VNHC on a physical testbed where $|I|$ must be large enough to overcome friction.

Setting $\bar{q}_a = 1$, we experimentally determined that $|I| = 10$ is a viable control parameter, so this is the value we will use for all simulations and experiments. In other words, the *injection* VNHC is (17) with $I = 10$ while the *dissipation* VNHC is (17) with $I = -10$.

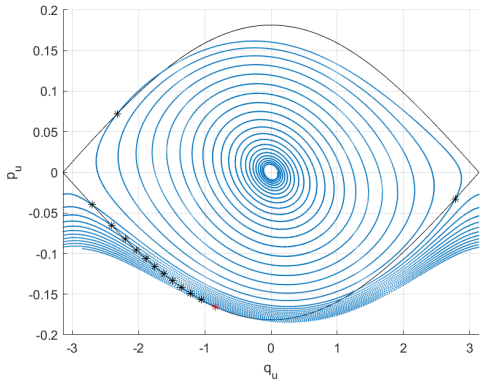

Fig. 5: A simulation of the acrobot gaining energy.

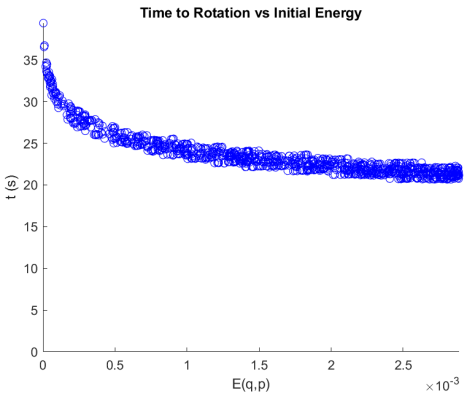

Fig. 6: Monte Carlo simulation for energy injection.

A. Energy Injection

In simulation, we stabilized the injection VNHC for the acrobot using the controller (14). We initialized the acrobot on the constraint manifold with initial condition $(q_u, p_u) = (\pi/32, 0)$ and simulated the constrained system for 30 seconds. The resulting orbit is plotted in Figure 5.

The level set $E_{\bar{R}}$, with $\bar{R} = E(\pi, 0)$, is outlined in black. Recall that this level set is the boundary between oscillations and rotations of the nominal pendulum. The points where the orbit exits $E_{\bar{R}}$ are marked with black asterisks, with the final departure marked by a red asterisk. Interestingly, the choice of I is large enough that we observe significant differences between the nominal pendulum and the constrained dynamics: $E_{\bar{R}}$ intersects the p_u-axis at $|p_u| \approx 0.17$, yet the constrained acrobot begins rotating once it hits the p_u-axis at $|p_u| \approx 0.16$. This indicates that higher values of I enable the acrobot to gain energy faster and begin rotating sooner, so long as the actuator does not saturate.

To verify numerically that the acrobot would consistently achieve rotations, we ran a Monte-Carlo [11] simulation where we initialized the acrobot randomly inside the sublevel set

$$\left\{(q_u, p_u) \in \mathbb{S}^1 \times \mathbb{R} \mid E(q_u, p_u) \leq E\left(\frac{\pi}{32}, 0\right)\right\},$$

and measured how long it took to begin rotating. The results in Figure 6 show that the acrobot always rotated within 20–40 seconds.

B. Energy Dissipation

In simulation, we stabilized the dissipation VNHC and initialized the acrobot on the constraint manifold with a rotation $(q_u, p_u) = (0, 0.18)$. We simulated the constrained system for 30 seconds and plotted the resulting orbit in Figure 7. As expected, the acrobot slows down over time. We highlight the locations where the orbit crossed the set $E_{\bar{R}}$ by black asterisks, with the final crossing in red. After this final crossing, the acrobot ceased rotating and its oscillations decayed to zero.

C. Oscillation Regulation

Recall from Section IV-B that one can use a supervisor to stabilize oscillations by appropriately toggling between injection and dissipation VNHCs whenever the orbit of the acrobot crosses the q_u-axis. Figure 8 shows the supervisor stabilizing an oscillation with body angle $q_{\text{des}} = \pi/2$ and a 5% hysteresis, meaning $\delta = 0.05$. The supervisor reevaluated its choice of VNHC at each black asterisk; the red contour corresponds to the part of the orbit where the supervisor kept the leg extended, because the oscillation was within tolerance of q_{des}. The solid black line is the desired oscillation, and the dashed black lines show the hysteresis around that orbit.

In Figure 8a the acrobot was initialized at $(q_u, p_u) = (\pi/32, 0)$; here the supervisor injected energy to stabilize the desired orbit. In Figure 8b the acrobot was initialized at the rotation $(q_u, p_u) = (0, 0.19)$; note that the supervisor is first

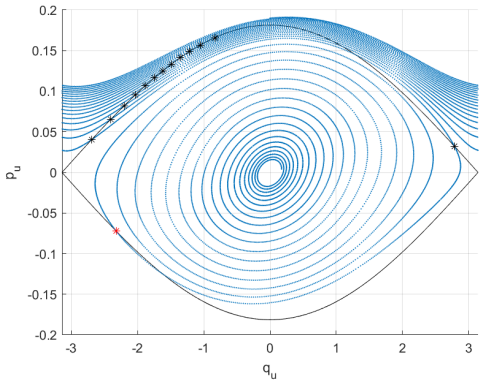

Fig. 7: A simulation of the acrobot dissipating energy.

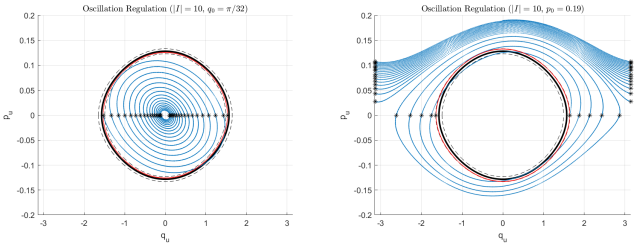

(a) Stabilizing an oscillation from below.

(b) Stabilizing an oscillation from above.

Fig. 8: Using a supervisor to stabilize the oscillation with peak angle $q_{\text{des}} = \pi/2$. The desired oscillation is depicted with a solid black line.

enabled at the line $|q_u| = \pi$ and dissipates energy. Eventually the acrobot begins a rocking motion and the supervisor is enabled again each time the acrobot hits the q_u-axis. The supervisor continues to dissipate energy until it stabilizes the desired oscillation.

D. Rotation Regulation

One can also use a supervisor to stabilize rotations through the mechanism described in Section IV-B, where the supervisor toggles between injection and dissipation VNHCs at each crossing of the p_u-axis. Rotation regulation for the acrobot is demonstrated in Figure 9, where the supervisor stabilizes $p_{\text{des}} = 0.19$ with a 2% hysteresis $\delta = 0.02$. The supervisor evaluated its choice of VNHC at each black asterisk. Once it was within range of p_{des} it extended the legs completely, the orbit of which is shown in red.

In Figure 9a the acrobot was initialized at the oscillation $(q_u, p_u) = (\pi/2, 0)$; here the supervisor injected energy until the orbit hit the p_u-axis near p_{des}. In Figure 9b the acrobot was initialized at the (fast) rotation $(q_u, p_u) = (0, 0.23)$; here the supervisor dissipated energy. In both cases, the desired rotation was stabilized correctly.

Note the difference in shape between the blue rotations of the dissipation VNHC and the red rotation of the nominal pendulum in Figure 9: the red one slows down much more near $|q_u| = \pi$. This difference arises because of the size of I: if $|I|$ were smaller, the blue rotations would be more similar in

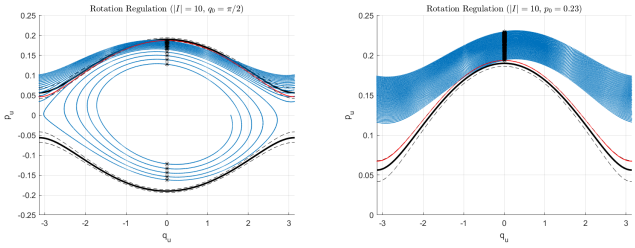

(a) Stabilizing a rotation from below.

(b) Stabilizing a rotation from above.

Fig. 9: Using a supervisor to stabilize the rotation with maximal momentum $p_{\text{des}} = 0.23$. The desired rotation is depicted with a solid black line.

shape to the red one because the constrained dynamics for the dissipation VNHC would be well approximated by the nominal pendulum.

E. Summary of Results

The simulation results in this section demonstrate the energy regulation capabilities of the proposed VNHC. We were able to stabilize both oscillations and rotations by implementing a control supervisor which toggled between injection, dissipation, and leg-extension VNHCs. In particular, these simulations indicate that the proposed VNHC works even for acrobots whose limbs have differing masses and lengths.

VI. Physical Experiments

A. Hardware Description

In this section we will demonstrate that the proposed VNHC is robust to friction, sensor noise, and other real-world considerations by testing it on the physical acrobot depicted in Figure 10. This platform is called SUGAR, which stands for Simple Underactuated Gymnastics and Acrobatics Robot. Its dynamic parameters are outlined in Table I.

SUGAR is comprised of two 3D-printed links: a torso and a leg. The torso houses an Arduino Nano microcontroller unit (MCU) which controls a Dynamixel RX24F servo motor between the torso and the leg. The MCU and the motor are powered by a 12V battery held in a compartment in the leg.

The torso is rigidly attached to a metal bar, which is held up by two wooden posts. On the exterior of one post is a control box with a power switch and a second Arduino Nano 328. The purpose of this control box is to read measurements from a rotary encoder connected to the metal bar, and to transmit these measurements to the MCU. The two Arduinos communicate through wires attached to a slip ring on the metal bar, and the signals are transmitted via I2C. The control box also provides a USB interface which allows the user to read the data from the acrobot in real time.

The rotary encoder directly measures q_u, and the Dynamixel servo motor provides measurements of q_a. However, there are no sensors measuring the velocity $\dot{q}$, which means we cannot directly evaluate p_u and p_a. To resolve this issue, the MCU estimates $\dot{q}$ by applying a washout filter to sequential

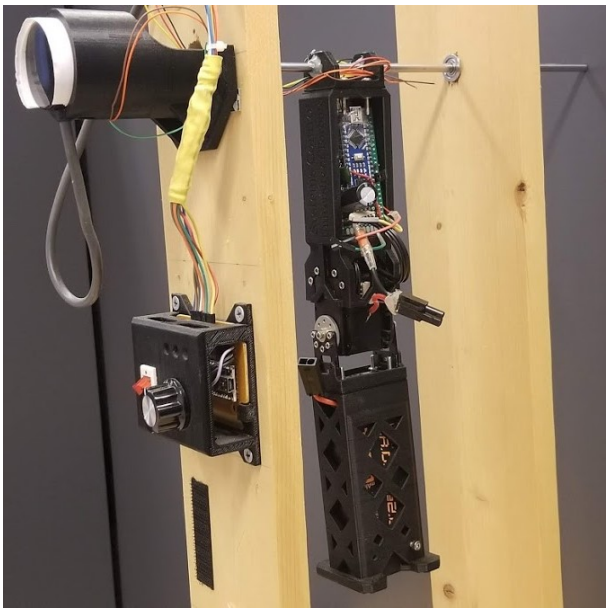

Fig. 10: SUGAR is the physical acrobot built by Wang [21].

measurements of q. We then compute $p = M(q)\dot{q}$ for use in the VNHC controller.

The communication speed between Arduinos restricts the sampling rate of p to 500Hz. This low sampling rate results in a noisy momentum signal which suffers from noticeable phase lag. This also rate-limits the control signal to 500Hz, which impacts any control implementation.

Finally, the Dynamixel servo motor does not have a torque control mode; instead, we can assign the servo setpoint at iteration $k \in \mathbb{Z}_{>0}$ via $q_a^k = \arctan(Ip_u^{k-1})$. This negatively affects the stabilization to the constraint manifold because we are introducing timing errors from the servo's built-in PID controller.

B. Experimental Results

We performed the following tests on SUGAR with the energy injection VNHC.

1) **Baseline Test:** we initialized SUGAR at $(q_u, p_u) \approx (\pi/8, 0)$. The resulting orbit in Figure 11 shows that SUGAR clearly gaining energy over time. Its motion looks similar to that of the energy injection simulation (Figure 5), though its energy gain ceases once it reaches a rotation with energy $E(0, 0.195)$. The energy gain likely ceases because of friction at the pivot, which was not modelled in simulation.
2) **Perturbation Test 1:** we initialized SUGAR at $(q_u, p_u) \approx (\pi, 0)$, let it run for 15 seconds, then introduced a rod as SUGAR passed through the bottom of its arc. This caused a collision which stopped SUGAR in its tracks, at which point we immediately removed the rod so SUGAR could continue unperturbed. The resulting orbit is shown in Figure 12. The blue rotation curve corresponds to the orbit before the disturbance, while the red spiral confirms that SUGAR begins oscillating after it was stopped. After the collision, SUGAR gains energy and eventually starts rotating again.
3) **Perturbation Test 2:** to see how SUGAR would respond when pushed, we allowed it to rotate unperturbed for 15 seconds and then pushed it in its direction of motion. The orbit in Figure 13a shows that SUGAR, when pushed, rotates with energy $E(0, -0.22)$, but then slows down until it reaches a rotation with energy $E(0, -0.195)$. We repeated this test by pushing SUGAR against its direction of motion. The orbit in Figure 13b demonstrates that SUGAR readily changes direction, and quickly achieves its maximum speed with energy $E(0, 0.195)$.

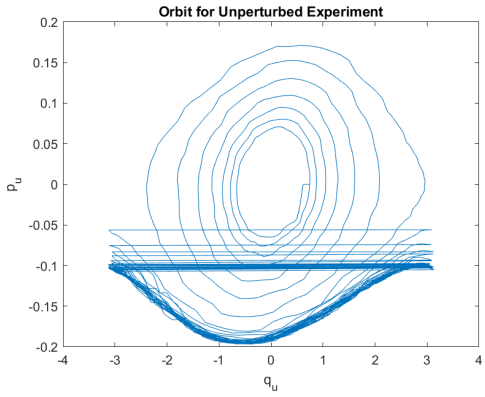

Fig. 11: Baseline Test: SUGAR's baseline energy injection orbit. A video of this experiment is available at `https://play.library.utoronto.ca/watch/6703e828acdcd38058ca884d13660a88`.

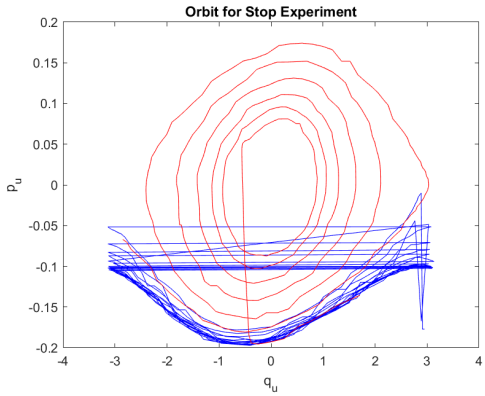

Fig. 12: Perturbation Test 1: SUGAR's orbit before (blue) and after (red) stopping. A video of this experiment is available at `https://play.library.utoronto.ca/watch/164a21f0a52d4d56ef60bf1911545e0e`.

In simulation, the acrobot was able to gain energy even when initialized with energy $E(q_u, p_u) > E(0, 0.195)$. The baseline and push tests suggest that the VNHC injects energy into SUGAR only on $\{E(q_u, p_u) \leq E(0, 0.195)\}$. This difference between simulation and implementation is likely due to friction, as well as timing errors incurred by the PID controller in the servo motor.

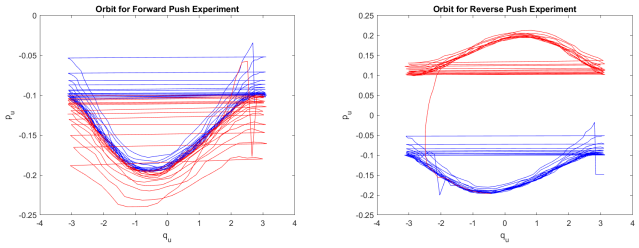

(a) The forward push test. (b) The reverse push test.

Fig. 13: Perturbation Test 2: SUGAR's orbit before (blue) and after (red) pushing. A video of this experiment is available at `https://play.library.utoronto.ca/watch/b13d4dc9f6daefa7f4d56dbf1b1bd482`.

C. Summary of Results

We performed three tests on SUGAR: a baseline energy injection test, a stop test, and a push test. These experiments demonstrate that VNHC-based energy injection is robust to significant model mismatch, friction, sensor noise, discretized control implementation, rate-limited measurement and control signals, and dramatic external disturbances.

VII. Proofs of Theorems 4 and 5

The proofs of the theorems rely on the next lemma.

Lemma 2: Let $\mathcal{U} \subset \mathbb{S}^1 \times \mathbb{R}$ be an open set and $R_2 > R_1 > 0$ be such that a connected component of $E_{[R_1,R_2]}$ is contained in $\mathcal{U}$. Let $T : \mathcal{U} \to \mathcal{V} :=]\underline{r}, \overline{r}[\times\mathbb{S}^1$, $(q_u, p_u) \mapsto (r, \theta)$, be a diffeomorphism such that

$$\begin{aligned} &\big(\forall R \in [R_1, R_2]\big)\big(\exists s \in]\underline{r}, \overline{r}[\big) \\ &T(E_R) = \{(r,\theta) \in \mathcal{V} : r = s\}, \end{aligned} \tag{21}$$

and the map $R \mapsto s$ is monotonically increasing. Suppose that $T : \mathcal{U} \to \mathcal{V}$ transforms system (18) into

$$\begin{aligned} \dot{r} &= f_r(r,\theta,I) \\ \dot{\theta} &= f_\theta(r,\theta,I), \end{aligned} \tag{22}$$

where f_r, f_θ and $g := f_r/f_\theta$ satisfy, for every $(r,\theta) \in \mathcal{U}$,

$$f_r(r,\theta,0) = 0, \;\; f_\theta(r,\theta,0) > 0, \tag{23a}$$

$$\partial_r g(r,\theta,0) = 0, \tag{23b}$$

$$\int_0^{2\pi} \partial_I g(r,\theta,I)\big|_{I=0} d\theta > 0. \tag{23c}$$

Then there exists $I^\star > 0$ such that for each $I \in]0, I^\star]$ (respectively, $I \in [-I^\star, 0[$) and every $x_0 \in E_{[R_1,R_2]} \cap \mathcal{U}$, the solution $x(t, x_0)$ enjoys the following properties:

(a) There exists $\bar{t} \geq 0$ such that $x(\bar{t}, x_0) \in E_{R_2}$ (respectively, E_{R_1}).

(b) If $R_2 < \bar{R}$, $x(t, x_0)$ is an oscillation gaining (respectively, losing) energy over $[0, \bar{t}]$. If $R_1 > \bar{R}$, $x(t, x_0)$ is a rotation gaining (respectively, losing) energy over $[0, \bar{t}]$.

Proof: By property (21), there exist $r_1, r_2 \in]\underline{r}, \overline{r}[$ such that $T(E_{[R_1,R_2]}) = [r_1, r_2] \times \mathbb{S}^1$. Moreover, $T(E_{R_2}) = \{r_2\} \times \mathbb{S}^1$. Define $K := [r_1, r_2] \times \mathbb{S}^1$, a compact subset of $\mathcal{V}$, and

$$b(r,\theta) := \partial_I g(r,\theta,I)\big|_{I=0}. \tag{24}$$

By properties (23a) and (23c) and since f_r, f_θ are continuous and K is compact, there exist $I_1, \varepsilon_1, \varepsilon_2 > 0$ such that for each $(r,\theta) \in K$ and $I \in [-I_1, I_1]$,

$$f_\theta(r,\theta,I) > \varepsilon_1, \tag{25a}$$

$$\int_0^{2\pi} b(r,\theta) d\theta > \varepsilon_2. \tag{25b}$$

Property (25a) implies that for $I \in [-I_1, I_1]$ the second component of any solution $(r(t), \theta(t))$ contained in K is a strictly monotonic function of t, and therefore $r(t)$ can be expressed as $r(t) = \hat{r}(\theta(t))$, where $\hat{r}(\theta)$ is a solution of

$$\frac{d\hat{r}}{d\theta} = g(\hat{r},\theta,I) = \frac{f_r(\hat{r},\theta,I)}{f_\theta(\hat{r},\theta,I)}. \tag{26}$$

Now let $\hat{r}(\theta, r_0, I)$ be the solution of (26) with initial condition $r(0) = r_0$ and $I \in [-I_1, I_1]$. The Taylor expansion of $\hat{r}(\theta, r_0, I)$ around $I = 0$ is

$$\begin{aligned} \hat{r}(\theta, r_0, I) &= \hat{r}(\theta, r_0, 0) + I\hat{r}_1(\theta, r_0) + \Delta(r_0, \theta, I) \\ &= r_0 + I\hat{r}_1(\theta, r_0) + \Delta(r_0, \theta, I), \end{aligned} \tag{27}$$

where the function $\Delta(r,\theta,I)$ is continuous and $I \mapsto \Delta(r,\theta,I)$ is $O(I^2)$. The second identity follows from the fact (due to (23a)) that $g(\hat{r},\theta,0) \equiv 0$. Following [8, Chapter 10], the function $\hat{r}_1(\theta, r_0)$ is the solution to the linear time-varying ODE

$$\begin{aligned} \frac{d\hat{r}_1}{d\theta} &= \partial_r g(r_0,\theta,0)\hat{r}_1 + b(r_0,\theta) \\ &= b(r_0,\theta), \end{aligned} \tag{28}$$

with initial condition $\hat{r}_1(0) = 0$. The second identity in (28) follows from (23b). We can solve (28) by quadrature, giving

$$\hat{r}_1(\theta, r_0) = \int_0^\theta b(r_0,\theta) d\theta. \tag{29}$$

Now consider the Poincaré section $\mathcal{P} = \{(r,\theta) \in \mathcal{V} : \theta = 0\}$. Using (27), and (29), the Poincaré map on $\mathcal{P}$ is $P : \mathcal{P} \to \mathbb{R}_{>0}$,

$$r \mapsto r + I \int_0^{2\pi} b(r,\theta) d\theta + \Delta(r, 2\pi, I). \tag{30}$$

Recall that $(r, I) \mapsto \Delta(r, 2\pi, I)$ is continuous and $O(I^2)$ for each fixed r. Since the set $[r_1, r_2] \times [-I_1, I_1]$ is compact, there exists $\kappa > 0$ such that $|\Delta(r, 2\pi, I)| \leq \kappa I^2$ for all $(r, I) \in [r_1, r_2] \times [-I_1, I_1]$. Using this inequality and property (25b) in (30), we get

$$\begin{aligned} \big(\forall I \in]0, I_1]\big) \;\; P(r) &> r + I\varepsilon_2 - \kappa I^2 \\ \big(\forall I \in [-I_1, 0[\big) \;\; P(r) &< r - |I|\varepsilon_2 + \kappa I^2, \end{aligned}$$

for all $r \in [r_1, r_2]$. Pick $I^\star \in]0, \min\{I_1, \varepsilon_2/\kappa\}[$ and let $\gamma := |I|\varepsilon_2 - \kappa I^2 > 0$. Then,

$$(\forall r \in [r_1, r_2])(\forall I \in]0, I^\star]) \;\; P(r) > r + \gamma \tag{31a}$$

$$(\forall r \in [r_1, r_2])(\forall I \in [-I^\star, 0[) \;\; P(r) < r - \gamma. \tag{31b}$$

Returning to the solution $\hat{r}(\theta, r_0, I)$ of (26), property (31a) implies that for each $(r_0, I) \in [r_1, r_2] \times]0, I^\star]$, there exists an integer $\bar{k} \geq 0$ such that the sequence $\{r(2\pi k, r_0, I)\}_{k=1,\ldots,\bar{k}}$ is monotonically increasing and $r(2\pi\bar{k}, r_0, I) \geq r_2$. Vice versa, property (31b) implies that for each $(r_0, I) \in [r_1, r_2] \times$

$[-I^\star, 0[$, there exists an integer $\bar{k} \geq 0$ such that the sequence $\{r(2\pi k, r_0, I)\}_{k=1,\dots,\bar{k}}$ is monotonically decreasing and $r(2\pi\bar{k}, r_0, I) \leq r_1$.

Now we return to system (22) with state (r, θ), and let $(r(t), \theta(t))$ be a solution initialized in K, with $0 < |I| \leq I^\star$. For $I > 0$ (respectively, $I < 0$), let $\bar{t} \geq 0$ be the first time such that $(r(\bar{t}), \theta(\bar{t})) \in \{r_2\} \times \mathbb{S}^1$ (respectively, $(r(\bar{t}), \theta(\bar{t})) \in \{r_1\} \times \mathbb{S}^1$). If the solution never intersects $\{r_2\} \times \mathbb{S}^1$, we set $\bar{t} = \infty$.

By property (25a), $\dot{\theta} > \varepsilon_1 > 0$, implying that the intersection of $(r([0, \bar{t}]), \theta([0, \bar{t}]))$ with $\mathcal{P}$ is a discrete set, and property (31) implies that the intersection points in $(r([0, \bar{t}]), \theta([0, \bar{t}])) \cap \mathcal{P}$ form a monotonically increasing (respectively, monotonically decreasing) sequence crossing the boundary $\{r_2\} \times \mathbb{S}^1$ (respectively, $\{r_1\} \times \mathbb{S}^1$) in finite time. This in turn implies that $\bar{t} < \infty$.

Returning to system (18) in original coordinates, we have shown that for each $x_0 \in E_{[R_1,R_2]} \cap \mathcal{U}$ and $0 < |I| \leq I^\star$, there exists $\bar{t} \geq 0$ such that the solution $x(t, x_0)$ enjoys these properties:

- For $I > 0$, $x(\bar{t}, x_0) \in E_{R_2}$, and for $I < 0$, $x(\bar{t}, x_0) \in E_{R_1}$.
- For $I > 0$, $x(t, x_0)$ is an oscillation or a rotation gaining energy over $[0, \bar{t}]$, depending on the values of R_1 and R_2. For $I < 0$, $x(t, x_0)$ is an oscillation or a rotation losing energy over $[0, \bar{t}]$.

This concludes the proof of Lemma 2. ∎

A. Proof of Theorem 4

We prove the theorem by producing a coordinate transformation $T : \mathcal{U} \to \mathcal{V}$ meeting the assumptions of Lemma 2. The transformation is adapted from [12].

Define $\mathcal{U} := E_{<\bar{R}} \setminus \{0\}$ and $\mathcal{V} :=]0, \pi[\times \mathbb{S}^1$, and consider the coordinate transformation[1] $T : \mathcal{U} \to \mathcal{V}$ defined as

$$\begin{aligned} T &: (q_u, p_u) \mapsto (r, \theta) \\ r &= \arccos\left(\cos(q_u) - \frac{p_u^2}{30m^2gl^3}\right) \\ \theta &= \arctan_2\left(-\operatorname{sgn}(p_u)\sqrt{1 - \frac{q_u^2}{r^2}}, \frac{q_u}{r}\right)\Bigg|_{r=r(q_u,p_u)}, \end{aligned} \tag{32}$$

whose inverse is

$$\begin{aligned} T^{-1} &: (r, \theta) \mapsto (q_u, p_u) \\ q_u &= r\cos(\theta) \\ p_u &= -\operatorname{sgn}(\sin(\theta))\sqrt{30m^2gl^3\cos(r\cos(\theta) - \cos(r))}. \end{aligned}$$

It is easily seen that for each $R \in]0, \bar{R}[$, $T(E_R) = \{(r, \theta) \in \mathcal{V} : r = \arccos(1 - R/(3mgl))\}$, and the function $R \mapsto \arccos(1 - R/(3mgl))$ is monotonically increasing. The diffeomorphism $T : \mathcal{U} \to \mathcal{V}$ therefore satisfies the first requirement of Lemma 2 for any choice of $0 < R_1 < R_2 < \bar{R}$.

In (r, θ) coordinates, T maps system (18) into a system of the form (22), where is straightforward to show that $f_r(r, \theta, 0) \equiv 0$ and

$$f_\theta(r, \theta, 0) = \sqrt{\frac{6g}{5l}}\sqrt{\frac{\cos(rc_\theta) - c_r}{r^2 s_\theta^2}}. \tag{33}$$

In the above we used the notation $c_\theta := \cos(\theta)$, $s_\theta := \sin(\theta)$, $c_r := \cos(r)$, and $s_r := \sin(r)$. We note that (33) has removable singularities at $\theta \in \{0, \pi\}$, since taking the limits as $\theta \to 0, \pi$ gives

$$\lim_{\theta\to 0} f_\theta(r, \theta, 0) = \lim_{\theta\to\pi} f_\theta(r, \theta, 0) = \sqrt{\frac{6gs_r}{10lr}}, \tag{34}$$

and these limits are smooth and well-defined for all $r \in]0, \pi[$. From (33)–(34), one can verify that $f_\theta(r, \theta, 0) > 0$ for all $(r, \theta) \in \mathcal{V}$, and thus assumption (23a) holds. Letting $g = f_r/f_\theta$, one can also verify that $\partial_r g(r, \theta, 0) \equiv 0$, and assumption (23b) holds. Symbolic computations reveal that $\partial_I g(r, \theta, I)\big|_{I=0} = La(r, \theta)$, where

$$\begin{aligned} L &:= \frac{\bar{q}_a\sqrt{30m^2gl^3}}{15}, \\ a(r, \theta) &:= \frac{r|s_\theta|\left(5c_r\cos(rc_\theta) - 8\cos(rc_\theta)^2 + 3\right)}{s_r\sqrt{\cos(rc_\theta) - c_r}}. \end{aligned}$$

Notice that L is a positive constant which depends only on

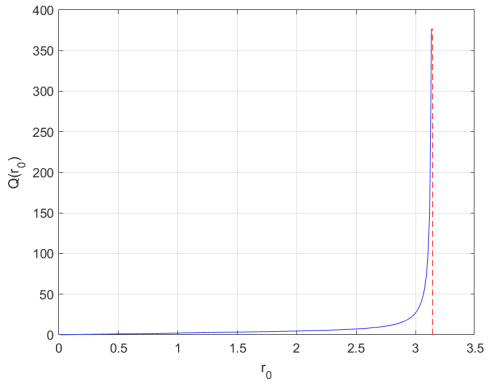

Fig. 14: The graph of $r \mapsto \int_0^{2\pi} a(r, \theta)d\theta$.

m, g, l, and $\bar{q}_a$, while $a(r, \theta)$ is adimensional. We have

$$\int_0^{2\pi} \partial_I g(r, \theta, I)\big|_{I=0} d\theta = L\int_0^{2\pi} a(r, \theta)d\theta.$$

The graph of $\int_0^{2\pi} a(r, \theta)d\theta$, shown in Figure 14, indicates that for each $r \in]0, \pi[$, the function $r \mapsto \int_0^{2\pi} a(r, \theta)d\theta$ is positive, and assumption (23c) holds. Thus the hypotheses of Lemma 2 are satisfied, proving the theorem. ∎

B. Proof of Theorem 5

We use again Lemma 2, this time producing two coordinate transformations, adapted from [12], whose domains are the two connected components of the set $E_{>\bar{R}}$.

Define $\mathcal{U}^+ := \left(E_{>\bar{R}}\right) \cap \{p_u > 0\}$, and $\mathcal{U}^- := \left(E_{>\bar{R}}\right) \cap \{p_u < 0\}$. Let $\mathcal{V} :=](10ml^2\bar{R})^{1/2}, \infty[\times \mathbb{S}^1$, and consider the

[1]Despite the presence of a sgn(·) function, this coordinate transformation T is actually smooth.

coordinate transformations $T^+ : \mathcal{U}^+ \to \mathcal{V}$ and $T^- : \mathcal{U}^- \to \mathcal{V}$ defined as

$$\begin{aligned} T^{\pm} &: (q_u, p_u) \mapsto (r, \theta) \\ r &= \sqrt{p_u^2 + 30m^2gl^3(1 - c_u)} \\ \theta &= \pm q_u, \end{aligned} \tag{35}$$

whose inverses are

$$\begin{aligned} (T^{\pm})^{-1} &: (r, \theta) \mapsto (q_u, p_u) \\ q_u &= \pm\theta \\ p_u &= \pm\sqrt{r^2 - 30m^2gl^3(1 - c_\theta)}. \end{aligned}$$

For each $R > \bar{R}$, it is easily seen that $T^{\pm}(E_R) = \{(r, \theta) \in \mathcal{V} : r = (10ml^2R)^{1/2}\}$, and the function $R \mapsto (10ml^2R)^{1/2}$ is monotonically increasing. Both T^+ and T^-, therefore, satisfy the first requirement of Lemma 2 for any $\bar{R} < R_1 < R_2$.

In (r, θ) coordinates, both T^+ and T^- map system (18) to a system of the form (22), where one can verify that $f_r(r, \theta, 0) \equiv 0$ and

$$f_\theta(r, \theta, 0) = \frac{1}{5ml^2}\sqrt{r^2 - 30m^2gl^3(1 - c_\theta)},$$

which is positive so assumption (23a) holds. Letting $g = f_r/f_\theta$, one can verify that $\partial_r g(r, \theta, 0) \equiv 0$, and assumption (23b) holds. The function $b(r, \theta) = \partial_I g(r, \theta, 0)$ is given in the statement of Theorem 5, and by assumption we have that condition (23c) of Lemma 2 holds. Theorem 5 now follows from Lemma 2 and the fact that $\mathcal{U}^+ \cup \mathcal{U}^- = E_{>\bar{R}}$. ■

VIII. Conclusion

In this article we applied the framework of virtual nonholonomic constraints to the acrobot, and designed a VNHC emulating giant motion from gymnastics. Our theoretical analysis applies to a simplified acrobot with point-mass limbs of equal length and mass, but the simulation and experimental results show the validity of the approach for a real acrobot. The main theoretical results of the paper, Theorems 4 and 5, assert that the proposed VNHC makes the dynamics of the acrobot on the constrained manifold gain or lose energy. There are two theoretical points that were unexplored in this paper. First, our analysis only considers initial conditions on the constraint manifold. For initial conditions off the manifold, there will be a transient whose effects we have not analyzed theoretically. Second, as pointed out in Remark 2, we have shown energy gain/loss of the constrained dynamics on compact subsets $E_{[R_1,R_2]}$ of $E_{<\bar{R}}$ and $E_{>\bar{R}}$, so both oscillations and rotations of the acrobot will gain/lose energy. We have not given theoretical guarantees that oscillations gaining energy eventually turn into rotations gaining energy. Both our simulations and the physical experiments suggest that our theoretical predictions continue to hold in the face of transients in enforcing the constraint, and that oscillations gaining energy will turn into rotations gaining energy.

References

[1] J. D. Castro-Díaz, P. Sánchez-Sánchez, A. Gutiérrez-Giles, M. Arteaga-Pérez, and J. Pliego-Jiménez, "Experimental results for haptic interaction with virtual holonomic and nonholonomic constraints," *IEEE Access*, vol. 8, pp. 120 959 – 120 973, July 2020.

[2] W. K. Chan, Y. Gu, and B. Yao, "Optimization of output functions with nonholonomic virtual constraints in underactauted bipedal walking control," in *2018 Annual American Control Conference*. Milwaukee, USA: IEEE, June 2018.

[3] G. Golub and W. Kahan, "Calculating the singular values and pseudo-inverse of a matrix," *Journal of the Society for Industrial and Applied Mathematics: Series B, Numerical Analysis*, vol. 2, no. 2, pp. 204–224, 1965.

[4] B. Griffin and J. Grizzle, "Nonholonomic virtual constraints for dynamic walking," in *2015 54th IEEE Conference on Decision and Control*. Osaka, Japan: IEEE, December 2015.

[5] T. Henmi, M. Chujo, Y. Ohta, and M. Deng, "Reproduction of swing-up and giant swing motion of acrobot based on a technique of the horizontal bar gymnast," in *Proceedings of the 11th World Congress on Intelligent Control and Automation*. Shenyang, China: IEEE, June 2014.

[6] J. Horn, A. Mohammadi, K. Hamed, and R. Gregg, "Hybrid zero dynamics of bipedal robots under nonholonomic virtual constraints," *IEEE Control Systems Letters*, vol. 3, no. 2, pp. 386 – 391, April 2019.

[7] J. C. Horn, A. Mohammadi, K. A. Hamed, and R. D. Gregg, "Nonholonomic virtual constraint design for variable-incline bipedal robotic walking," *IEEE Robotics and Automation Letters*, vol. 5, pp. 3691 – 3698, February 2020.

[8] H. K. Khalil, *Nonlinear Systems*, 3rd ed. Upper Saddle River, NJ 07485: Prentice Hall, 2002.

[9] L. D. Landau and E. M. Lifschitz, *Mechanics*, 3rd ed. Butterworth-Heinemann, January 1982.

[10] M. Maggiore and L. Consolini, "Virtual holonomic constraints for euler-lagrange systems," *IEEE Transactions on Automatic Control*, vol. 58, no. 4, pp. 1001 – 1008, April 2013.

[11] N. Metropolis, "The beginning of the monte carlo method," *Los Alamos Science*, pp. 125–130, 1987, 1987 special issue dedicated to Stanislaw Ulam.

[12] A. Mohammadi, M. Maggiore, and L. Consolini, "Dynamic virtual holonomic constraints for stabilization of closed orbits in underactuated mechanical systems," *Automatica*, vol. 94, pp. 112 – 124, August 2018.

[13] K. Ono, K. Yamamoto, and A. Imadu, "Control of giant swing motion of a two-link horizontal bar gymnastic robot," *Advanced Robotics*, vol. 15, no. 4, pp. 449 – 465, 2001.

[14] E. Papadopoulos and G. Papadopoulos, "A novel energy pumping strategy for robotic swinging," in *2009 17th Mediterranean Conference on Control and Automation*. Thessaloniki, Greece: IEEE, June 2009.

[15] P. E. Pidcoe, "The biomechanics principles behind training giant swings," Online, Virginia Commonwealth University, Richmond, VA, USA, August 2005, accessed 11 September 2020. https://usagym.org/pages/home/publications/technique/2005/8/giant.pdf.

[16] R. D. Schafer, *An Introduction to Non-Associative Algebras*. New York: Dover Publications, 1996.

[17] V. Sevrez, E. Berton, G. Rao, and R. J. Bootsma, "Regulation of pendulum length as a control mechanism in performing the backward giant circle in gymnastics," *Human Movement Science*, vol. 28, no. 2, pp. 250 – 262, March 2009.

[18] S. Shibata and T. Murakami, "Psd based virtual nonholonomic constraint for human interaction of redundant manipulator," in *Proceedings of the 2004 IEEE International Conference on Control Applications*. Taipei,Taiwan: IEEE, September 2004.

[19] T. Takubo, H. Arai, and K. Tanie, "Virtual nonholonomic constraint for human-robot cooperation in 3-d space," in *2000 IEEE/RSJ International Conference on Intelligent Robots and Systems*. Takamatsu, Japan: IEEE, October 2000.

[20] S. Vozar, Z. Chen, P. Kazanzides, and L. L. Whitcomb, "Preliminary study of virtual nonholonomic constraints for time-delayed teleoperation," in *2015 IEEE/RSJ International Conference on Intelligent Robots and Systems*. Hamburg, Germany: IEEE, October 2015.

[21] X. Wang, "Motion control of a gymnastics robot using virtual holonomic constraints," Master's thesis, University of Toronto, 2016.

[22] S. Wirkus, R. Rand, and A. Ruina, "How to pump a swing," *The College Mathematics Journal*, vol. 29, no. 4, pp. 266 – 275, 1998.

[23] X. Zhang, H. Cheng, Y. Zhao, and B. Gao, "The dynamical servo control problem for the acrobot based on virtual constraints approach," in *The 2009 IEEE/RSJ International Conference on Intelligent Robots and Systems*. St. Louis, USA: IEEE, October 2009.